Phys. Status Solidi C **14,** No. 7, 1700074 (2017) / **DOI** 10.1002/pssc.201700074

physica status solidi c
www.pss-c.com
current topics in solid state physics

Dislocation trails in Si: Geometry and electrical properties

V. I. Orlov[*,1,2], **E. B. Yakimov**[1,3], **and N. Yarykin**[1]

[1] Institute of Microelectronics Technology RAS, 142432 Chernogolovka, Russia
[2] Institute of Solid State Physics RAS, 142432 Chernogolovka, Russia
[3] National University of Science and Technology MISiS, 119049 Moscow, Russia

Received 3 February 2017, accepted 18 April 2017
Published online 16 May 2017

Keywords dislocation trails, EBIC, LBIC, plastic deformation, silicon

* Corresponding author: e-mail orlov@issp.ac.ru, Phone: 8 985 7875899, Fax: 8 (496) 522 8160

Dislocation trails, the quasi-2D defects left behind gliding dislocations, are studied in terms of the dislocation motion geometry. The individual dislocation half-loops are introduced in silicon crystals at 600 °C from the sources on the tensile {100} surface. The electrically active dislocations and dislocation trails are revealed by their recombination activity using the LBIC and EBIC techniques. It is found that only one 60° segment of the dislocation half-loop creates the dislocation trail, while the screw and differently aligned 60° segments do not. Reversal of the dislocation motion is observed to alternate the role of the 60° segments in the dislocation trail formation. All results are consistent with the model which assumes that the electrically active dislocation trails are created by the dissociated 60° dislocation with the 90° leading partial.

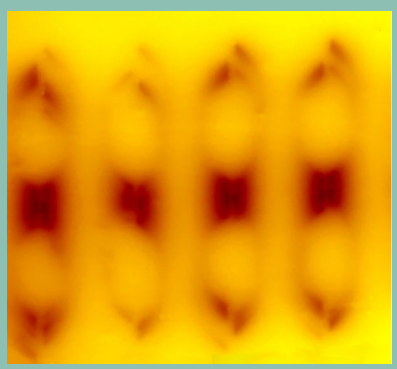

LBIC image of the defects formed by expansion of the dislocation half-loops created from the tensile {100} silicon surface.

1 Introduction In some cases, *gliding* dislocations in silicon leave behind a somehow disturbed crystal and thus form a quasi-two-dimensional defects in the immediate vicinity of the slip plane, the dislocation trails (DTs). DTs were first revealed by the selective chemical etching [1–5]. Later on, the dislocation trails were observed to be electrically active that allows their detection by electrical methods. It was found that DTs induce the conductivity anisotropy [2, 3], introduce deep levels [6, 7], and can be visualized by their recombination activity using the electron- and laser-beam induced current methods (EBIC and LBIC, respectively) [4, 6, 8, 9]. The microscopic nature of dislocation trails and the mechanisms of their generation are not clear up to now, although influence of the impurity contents and the deformation conditions were noted [3, 10].

One of the puzzling features of the dislocation trails is an apparent irregularity of their appearance as revealed by comparison of different reports. In part, the scattering of experimental data could be understood taking into account that the DT etching patterns vary with a distance from the sample surface and differ in the regions subjected to the tensile or compressive deformations [8, 9]. In attempt to realize this irregularity, it was proposed that the dislocation trails are formed only behind the 60° dislocations [4, 5]. However, it has been recently demonstrated that not all 60° segments generate the trails [8, 9]. Most of observed results conform to the assumption that the ability to generate the

trails depends on the order of partials in dissociated 60° dislocation [9]. In this work, we continue this analysis including the new results obtained by the EBIC and LBIC methods on the silicon samples deformed in different geometries.

2 Experimental The experiments were performed on the dislocation-free Cz–Si single crystals of p-type ([B] $\sim 10^{15}\,cm^{-3}$). The samples for plastic deformation were cut in the form of rectangular bars of the $35 \times 4 \times 0.7\,mm^3$ dimensions with the long edge along a <110> direction and the wider face parallel to a {100} plane. To remove the unwanted dislocation sources, the bars were chemically polished. Instead, the controllable dislocation sources were created by a diamond indenter at room temperature. The bars were then stressed at 600 °C in the four-point bending geometry with the <110> bend axis. Accordingly, the compressive and tensile stresses were applied to the upper and lower parts of the sample, respectively. The sign of the stress can be alternated for each dislocation loop by turning the sample upside-down. After the deformation, a 100 μm thick layer was etched out from all faces. In particular, this minimized an effect of the dislocation near-surface bending.

Dislocations and dislocation trails were revealed by Nomarsky optical microscope after treatment in Sirtle etchant. For EBIC and LBIC measurements, the semi-transparent Schottky diodes were formed by evaporation of aluminum and ohmic contacts were produced by rubbing with Al–Ga eutectic. The EBIC studies were carried out in the JSM-840 scanning electron microscope at room temperature. Usually, the beam energy and current were of 35 keV and 10^{-10} A, respectively. The LBIC measurements were carried out at room temperature using a homemade setup on the base of an optical microscope and the computer-controlled x-y stage. A semiconductor laser with a 980 nm wavelength and a power of 20 mW was used as an excitation source. The penetration depth of the laser beam was about 150 μm that allows obtaining quasi-3D images of the inclined dislocations and dislocation trails.

The recombination contrast of DT is known to decrease with excitation level increasing [4]. Excitation level in the LBIC measurements is usually higher than that in the EBIC method. On the other hand, the LBIC sensitivity is higher for uncharged two-dimensional defects. Therefore, it is useful to apply both methods to the same samples for reliable defect detection.

3 Results and discussion Figure 1 represents the EBIC and LBIC images obtained from the same region of the tensile {100} face where the defects were generated from four dislocation sources. Before going into details of the pictures, let us consider the geometry of defects created by a single dislocation source (Fig. 1c). The source located in the middle of the sketch generates dislocation half-loops which expand in two inclined {111} slip planes. In the used deformation geometry, the bottom segments of the half-loops are always of the 60° type, while the screw segment can be located either in the upper or bottom part of the sketch with equal probability. The part of slip plane swept by the bottom segment of half-loop (shown in gray in Fig. 1c) is limited to a relatively small central region. Indeed, the bottom dislocation segment is located at the depth of ~200 μm in our samples. This is because the acting stress is reduced to zero in the middle of a bent bar. When the bottom segment reaches the maximum depth, size of the half-loop is expected to be about 600 μm. Therefore, further expansion of the half-loop (up to 1500 μm as seen in Fig. 1a and b) proceeds by movement of the side arms (which intersect the surface) and by elongation of the bottom segment. As a result, the greater part of the slip plane is swept by the side arms.

Returning to Fig. 1a and b, note that the EBIC and LBIC images are essentially different. Only the points where the side arms intersect the surface are seen in the EBIC mode as dark spots (dark arrows in Fig. 1a), while the whole dislocation half-loops are revealed by the LBIC technique. This difference is determined by the dissimilar excitation depths in these two methods: The laser beam penetration length is comparable to the depth where the bottom segments are

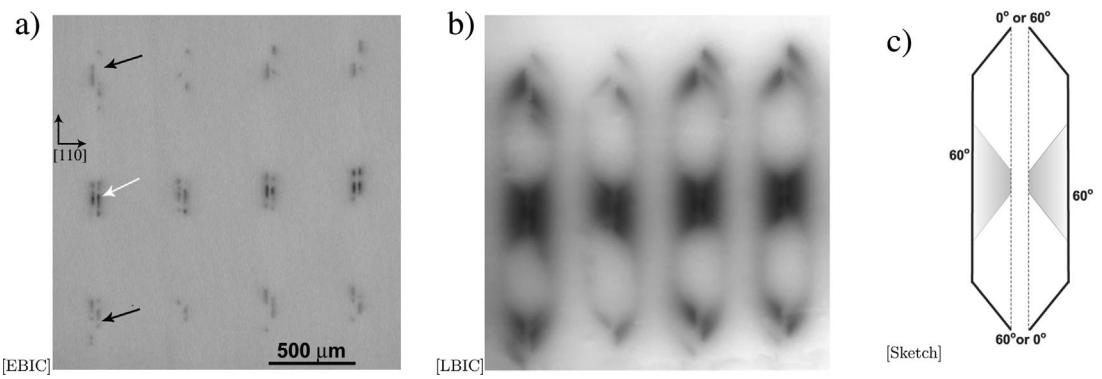

Figure 1 The EBIC (a) and LBIC images (b) obtained from the same area of the {100} surface after deformation under the tensile stress and the schematic representation of the dislocation half-loops and dislocation trails (c) in projection on the {100} surface of observation.

located, while the electron beam excites only a ~15 μm near-surface layer.

Both methods reveal also an additional contrast in the middle of half-loops (bright arrow in Fig. 1a) which we ascribe to the dislocation trails created by the bottom segment. This conclusion is supported by a good correlation of the shape of LBIC contrast in Fig. 1b with the form of the gray region in Fig. 1c. Other parts of the slip plane swept by the side arms do not reveal any presence of dislocation trails. Thus, the detectable dislocation trails are produced in the given deformation geometry by the bottom 60° segment only.

These observations and those obtained earlier on the samples with the {111} working surface [9], lead us to the conclusion that two differently aligned 60° segments behave differently. Our analysis shows that this non-equivalence could be related to a different order of partials in the dissociated 60° dislocation. Let us consider the half-loop expanded from the tensile {100} surface. According to [11], the dissociated bottom segment has always the 90° leading partial independent of which of two possible Burgers vectors is realized, while the side arms have always the 30° leading partials. Thus we infer that the dislocation trails are only formed by those 60° dislocation segments for which the leading partials are of the 90° type.

The order of partials can be changed just by reversing the direction of dislocation motion. For example, the 60° side arm will always has the 90° leading partial during shrinking the half-loops shown in Fig. 1. The LBIC image of such shrunk half-loops is shown in Fig. 2. First, the dislocation half-loops were introduced from the tensile {100} surface. The loop size was ~500 μm as obtained by the selective chemical etching (dark arrows in Fig. 2). Then the sample was loaded again in such a way that the former tensile surface gets compressed. Stress and time for the reversal movement were chosen to provide the half-loops of a minimum final size (<50 μm).

It is seen in Fig. 2 that the LBIC contrast (bright arrows) is revealed at the distance up to ~200–250 μm from the center which is much longer than the final half-loop size. Taking into account that no LBIC contrast is produced by the side arms during the direct dislocation motion (see Fig. 1), we conclude that the obtained dislocation trails are formed during the half-loop shrinking. The EBIC studies show similar results except the quasi-three-dimensional imaging.

Figure 2 demonstrates also that only one side arm in each half-look forms the LBIC contrast during the reversal dislocation motion, while the other arm does not. This conforms with our model [9] that only the 60° dislocations with the 90° leading partials are able to create the dislocation trails.

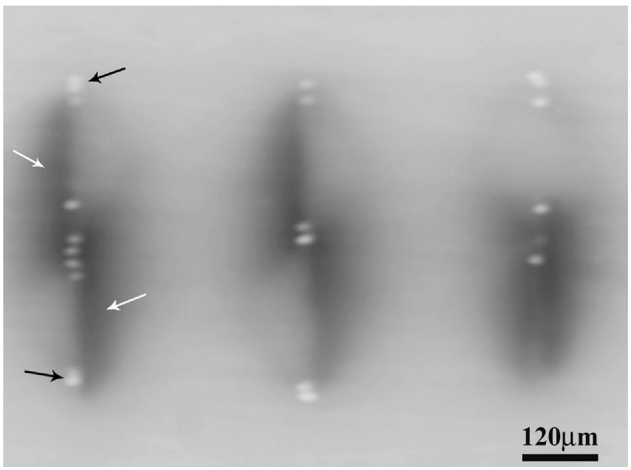

Figure 2 LBIC image of the dislocation trails formed by shrinking the dislocation half-loops under compressive stress after the initial expansion from the tensile {100} surface.

4 Conclusions In the present work, using the samples with different crystallographic orientation, we reconfirm our earlier result that the dislocation trails are formed behind only one segment of the dislocation half-loop. This is always the 60° segment which, if dissociated, has the 90° leading partial. The additional argument in support of this model is obtained in this work by changing the order of partials by reversing the direction of dislocation motion. It is observed that the segment, which was inactive in the DT formation during the expansion of dislocation half-loop, gets active when the the dislocation loop starts to shrink.

References

[1] W. C. Dash, J. Appl. Phys. **29**, 705 (1958).
[2] V. G. Eremenko, V. I. Nikitenko, and E. B. Yakimov, JETP Lett. **26**, 65 (1977).
[3] I. Bondarenko, V. G. Eremenko, B. Farber, V. I. Nikitenko, and E. B. Yakimov, Phys. Stat. Sol. (a) **68**, 53 (1981).
[4] I. Bondarenko, H. Blumtritt, J. Heydenreich, V. V. Kazmiruk, and E. B. Yakimov, Phys. Stat. Sol. (a) **95**, 173 (1986).
[5] V. G. Eremenko, J. L. Demenet, and J. Rabier, Phys. Stat. Sol. C **6**, 1801 (2009).
[6] I. Bondarenko, E. B. Yakimov, and N. A. Yarykin, Acta Phys. Polonica A **69**, 393 (1986).
[7] O. V. Feklisova, E. B. Yakimov, and N. Yarykin, Physica B **340–342**, 1005 (2003).
[8] O. V. Feklisova, V. I. Orlov, and E. B. Yakimov, Phys. Stat. Sol. C **12**, 1081 (2015).
[9] V. I. Orlov, E. B. Yakimov, and N. Yarykin, Solid State Phenom. **242**, 155 (2016).
[10] V. Kveder, M. Khorosheva, and M. Seibt, Solid State Phenom. **242**, 147 (2016).
[11] J. P. Hirth and J. Lothe, Theory of Dislocations (John Wiley & Sons, New York, Chichester, Brisbane, Toronto, Singapore, 1982), p. 319.